International Journal of Basic and Applied Sciences, 14 (6) (2025) 169-181

International Journal of Basic and Applied Sciences

Website: www.sciencepubco.com/index.php/IJBAS
https://doi.org/10.14419/z35t2r98
Research paper

Synchronization and Chaotic Dynamics of A Josephson Junction Shunted by A Negative Conductance

G. F. Pomalegni [1,3], M. A. Kakpo [2,3,4], C. H. Miwadinou [2,3,4,5,*]

[1] École de Génie Rural, Université Nationale d'Agriculture, Kétou, Bénin
[2] École Doctorale Sciences, Technologies, Ingénierie et Mathématiques (ED-STIM) ; Université Nationale des Sciences, Technologies, Ingénierie et Mathématiques (UNSTIM)
[3] Laboratoire de Mécanique des Fluides, de la Dynamique Nonlinéaire et de la Modélisation des Systèmes Biologiques (LMFDNMSB); Institut de Mathématiques et de Sciences Physiques, Porto-Novo, Bénin
[4] Laboratoire de Physique et Applications (LPA) du Centre Universitaire de Natitingou,Université Nationale des Sciences, Technologiques, Ingénierie et Mathématiques (UNSTIM)Abomey, Bénin
[5] Département de Physique, Chimie et Technologie, École Normale Supérieure de Natitingou, Université Nationale des Sciences, Technologiques, Ingénierie et Mathématiques (UNSTIM) Abomey,Bénin
**Corresponding author E-mail: clement.miwadinou@imsp-uac.org*

Received: July 11, 2025, Accepted: August 26, 2025, Published: October 9, 2025

Abstract

This paper presents a theoretical and numerical investigation of the RCLSJ model (Resistively, Capacitively, and Inductively Shunted Junction), which is described by a nonlinear current source characterized by the current-phase relationship I_O (sinØ-α_1 sin2Ø+α_2 sin3Ø), coupled with a negative conductance. The rate equations governing the RCLSJ model reveal that, depending on the parameter regions, the system may either lack fixed points entirely or possess two or four fixed points. These regions are determined by the intensity of the negative conductance and the second-order harmonic term, under the assumption of a normalized critical current. Our analysis demonstrates that the presence of negative conductance suppresses certain hidden dynamical orders associated with periodic instabilities. Furthermore, the introduction of the third-order harmonic term significantly alters the nonlinear dynamics of the RCLSJ system. In addition, master-slave synchronization studies indicate that the third-order harmonic modifies synchronization frequencies by generating new resonance modes. For specific threshold values of α2, it enhances synchronization, while variations in the intensity of the negative conductance lead to higher-frequency oscillations. These different influences induced by the negative conductance and the third-order harmonic term of the junction suggest that the system could be used in the superconducting circuits for qubits, synchronized oscillators for the generation of THz signals, and also in computational neuroscience.

Keywords: *Bifurcation and Chaos; Josephson Junction; Negative Conductance; Intermittency; Synchronization.*

1. Introduction

A Josephson junction is a highly nonlinear component commonly used in applications requiring minimal power consumption, including quantum bit implementation and microwave photonics [1], [2]. It is made up of two superconductors separated by a thin insulating barrier. When this barrier is sufficiently thin, a supercurrent can pass through the junction without any applied voltage, a phenomenon known as the Josephson effect. This effect enables the use of Josephson junctions in superconducting quantum interference devices (SQUIDs) for detecting extremely weak magnetic fields [3]. Early studies, such as those by Belykh et al [4], [5], highlighted the complex dynamic behavior of the Josephson junction. Later, in 1980, Crutchfield et al [6] constructed numerical investigations into chaotic behavior within Josephson junctions (JJs). To model these phenomena, several approaches were developed, including linear and nonlinear (piecewise linear) resistive-capacitive shunted JJ models [7], [8], and more advanced linear and nonlinear Resistive-Capacitive-Inductive Shunted JJ (RCISJJ) models [9-12]. The control and synchronization of the chaotic dynamics of Josephson junctions have relied on several methods, including sliding mode control [13, 14], backstepping control [15], Lyapunov direct method, and others. The synchronization of the non-linear dynamics of the Josephson junction with a third-order harmonic term is a subject of study in the physics of superconductors and in the dynamics of nonlinear systems. Synchronization in nonlinear dynamics causes a system to respond to an external excitation coherently, adopting a frequency linked to that of the excitation. In the third-order harmonic term Josephson junction used in this paper, the dynamics of the phase frequency of the junction display a synchronous behavior under the effect of the alternating current signal used. The presence of the third-order harmonic term modifies the resonance conditions and generates a shift in the synchronization frequencies, the appearance of new synchronous modes, and a transition towards chaotic behavior. All these observed behaviors differ from those obtained in [16] when the same junction is studied without the harmonic term of order three. Master-slave synchronization is a phenomenon where a

nonlinear system (slave) follows the dynamics of another system (master) under certain coupling conditions. Master-slave synchronization has been successfully applied to several Josephson junctions [17], [18]. In the case of a Josephson junction with an order-three harmonic term, the phase and frequency of the oscillations of the slave junction align with those of the master. The presence of the term α2sin3x modifies the synchronization frequency, stabilizes the synchronous regime, and promotes nonlinear effects in the phase-locking dynamics. The study of chaos in Josephson junctions with a third-order harmonic term coupled to a negative conductance relates to nonlinear dynamic systems and chaotic effects in superconducting circuits. A negative conductance means that the derivative is negative, which can appear in certain nonlinear electronic systems (tunnel diodes, unconventional superconductors, active circuits). This can induce an amplification of oscillations, trigger dynamic instability leading to chaotic behavior, and modify oscillations by introducing bifurcations. The study of synchronization in modified junctions is essential for superconducting qubits, where the presence of a modified nonlinear term can influence coherence times and quantum operations. In superconducting materials, higher-order harmonic Josephson junctions are used to manipulate electromagnetic waves, and these junctions are also used in superconducting oscillators that exploit nonlinear dynamics for applications in signal detection or generation. In the literature, several works have been carried out on the different types of superconducting structures that contain a second-order harmonic term in the form of $I_c$sinx- αI_c sin2x, where Ic is the critical current of the junction and α is the second-harmonic parameter [19]. The great importance of the influence of the second harmonic term of the Josephson junction has been extensively studied in the literature.

This work highlights, through complementary experimental and theoretical approaches, the central role of negative conductance in controlling and tailoring superconducting states. The experimental study on $NbSe_2$ thin films [20] under surface acoustic wave (SAW) irradiation demonstrates the feasibility of inducing a negative resistance within the superconducting gap via dynamic modulation of the charge density wave. This provides direct evidence that out-of-equilibrium interactions can invert the voltage-current relationship, offering a novel route for precise tuning of superconducting transport properties. In parallel, the theoretical and numerical analysis of the RCLSJ model with higher-order harmonics shows that negative conductance can profoundly reshape system dynamics: altering the number and stability of fixed points, suppressing unstable periodic regimes, generating new resonance modes, and enhancing synchronization. The experimental observations in $NbSe_2$ can thus be interpreted as a tangible realization of effects predicted by the RCLSJ model, while the latter provides a predictive framework to guide and optimize future experiments. Together, these results not only pave the way for the design of multifunctional superconducting circuits but also reveal a previously unexplored mechanism for out-of-equilibrium control of superconductivity, with promising applications in THz signal generation, quantum information processing, and neuromorphic computing. Articles [21] and [22] investigate third-harmonic generation (THG) in superconductors under intense THz excitation, where the THG arises from nonlinear interactions between quasiparticles and collective modes (notably the Higgs amplitude mode) and is strongly influenced by disorder. The third harmonic here emerges as a phenomenon induced by the external driving field. This paper, on the other hand, introduces an intrinsic third-harmonic term ($\alpha_2$sin3φ) directly into the current-phase relation of a modified RCLSJ Josephson junction. This structural nonlinearity alters dynamic stability, generates new resonance frequencies, and enhances oscillator synchronization, providing a direct parametric control. Thus, while articles [21] and [22] treat the third harmonic as a signature of nonlinear response, this paper integrates it as a fundamental control tool for superconducting dynamics and THz applications. The experimental realization of negative conductance in superconducting circuits faces challenges related to stability, precise control of active components, and cryogenic compatibility. Incorporating a third-order harmonic term also requires fine-tuning of the Josephson junction's nonlinear properties, involving advanced fabrication techniques. These phenomena directly impact superconducting qubit performance, particularly coherence times, as well as the spectral purity of THz signals. Thus, mastering parameter ranges and damping mechanisms is crucial to harnessing these nonlinear effects for practical applications. Despite the different aspects of the chaotic dynamics of the junctions Josephson addressed in the literature, the study of junctions Synchronization of the chaotic dynamics of a Josephson junction with a third-order harmonic term coupled to a negative conductance has not yet been addressed. Josephson with a harmonic term of order three coupled with a negative conductance has not yet been addressed. This is the reason why we have produced such a model in order to show the influence of negative conductance on the circuit and then show that the third-order harmonic term modifies the nonlinear dynamics of the Josephson junction by favoring a modification of the synchronization frequencies, the appearance of new synchronous modes. The remainder of this paper is organized as follows: Section 2 introduces the circuit model and its governing equations. Section 3 discusses the analytical and numerical analysis. Section 4 presents the numerical simulations. Section 5 addresses the synchronization study, and Section 6 concludes the work.

2. Model and Equation of Oscillations

The circuit in Figure 1 consists of an external alternating voltage source, a nonlinear Josephson junction characterized by a supercurrent of the form $I_O(\sin\emptyset - \alpha_1 \sin 2\emptyset + \alpha_2 \sin 3\emptyset)$, a passive RL element carrying the current I_S, and a negative conductance gn is introduced into the system. The nodal equation at the junction, Kirchhoff's loop law, and the voltage-phase relationship.

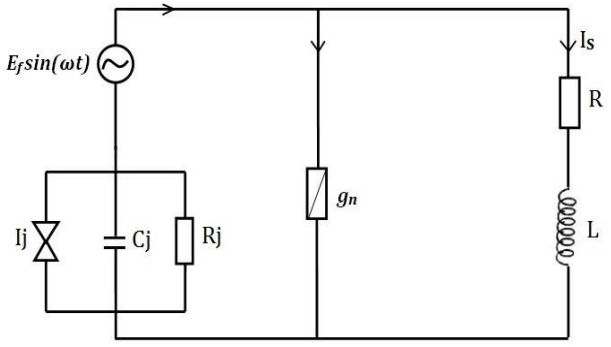

Fig. 1: Circuit of the Model Studied.

The nodal equation at the junction, Kirchhoff's loop law, and the voltage-phase relationship specific to the Josephson junction together form the governing equation of the circuit.

$$\begin{cases} I_O(\sin\emptyset - \alpha_1 \sin 2\emptyset + \alpha_2 \sin 3\emptyset) + C_j \frac{dV_j}{dt} + \frac{V_j}{R_j} = I_g + I_S' \\ E_f \sin(wt) = RI_s + L\frac{dI_s}{dt} + V_j' \\ V_j = \frac{\hbar}{2e}\frac{d\emptyset}{dt}, \end{cases} \quad (1)$$

A group of dimensionless variables and parameters is defined by:

$$\begin{cases} x = \emptyset' \\ y = \frac{I_s}{I_o}, \\ z = \frac{V_J}{RI_O}, \end{cases} \quad (2)$$

The system under investigation is described by the following set of differential equations:

$$\begin{cases} \dot{x} = z, \\ \dot{y} = \frac{E_f}{\gamma}\sin(wt) + \frac{1}{\xi}(-z - y)' \\ \dot{z} = \frac{I}{\varepsilon}\left(y - \tau(z)z - \sin(x) + \alpha_1 \sin(2x) - \alpha_2 \sin(3x) + \frac{I_g}{I_0}\right)' \end{cases} \quad (3)$$

With

$$\begin{cases} \gamma = LI_0' \\ \xi = \frac{L}{R}, \\ \varepsilon = C_j R' \end{cases} \quad (4)$$

$$\tau(z) = \begin{cases} 0.366 \text{ if } |z| > 2.9 \\ 0.061 \text{ if } |z| \leq 2.9 \end{cases} \quad (5)$$

3. Equilibrium Points

This section focuses on identifying the constant values of the dynamic variables for which all time derivatives vanish, assuming the external source $E_f \sin(wt)$ is not present. This leads us to the following analysis:

$$\begin{cases} \frac{I_g}{I_0} - \sin(x^*) + \alpha_1 \sin(2x^*) - \alpha_2 \sin(3x^*) = 0, (a) \\ y^* = 0, (b) \\ z^* = 0, (c) \end{cases} \quad (6)$$

The fixed point E (x^* ; 0; 0) of system (3) is therefore defined by an algebraic equation on the phase: $\frac{I_g}{I_0} - \sin(x^*) + \alpha_1 \sin(2x^*) - \alpha_2 \sin(3x^*) = 0$. The equation has several solutions depending on the parameters $I_g, I_0, \alpha_1, \alpha_2$, which induces multistability. The fixed points can be stable or unstable, depending on the derivative of the nonlinear term with respect to x^*. (as shown in Figure 2a). The characteristic polynomial of the system (3) evaluated at the fixed-point E is given by:

$$\lambda^3 + \left(\frac{1}{\xi} + \frac{b_1}{\varepsilon}\right)\lambda^2 + \left(\frac{b_1+1}{\xi\varepsilon} + \frac{\text{Cos}x^* - 2\alpha_1 \text{cons}2x^* + 3\alpha_2 \text{sin}3x^*}{\varepsilon}\right)\lambda + \frac{(\text{Cos}x^* - 2\alpha_1 \text{cons}2x^* + 3\alpha_2 \text{sin}3x^*)}{\xi\varepsilon} = 0 \quad (7)$$

Setting

$$\begin{cases} a_1 = \frac{1}{\xi} + \frac{b_1}{\varepsilon}, \\ a_{2=\frac{b_1+1}{\xi\varepsilon} + \frac{\text{Cos}x^* - 2\alpha_1 \text{cons}2x^* + 3\alpha_2 \text{sin}3x^*}{\varepsilon}}, a_3 = \frac{\text{Cos}x^* - 2\alpha_1 \text{cons}2x^* + 3\alpha_2 \text{sin}3x^*}{\xi\varepsilon}, \end{cases} \quad (8)$$

With $b_1 = \tau(z)$.

The eigenvalue equation becomes:

$$\lambda^3 + a_1\lambda^2 + a_2\lambda + a_3 = 0 \quad (9)$$

Based on the Routh-Hurwitz criterion, all the roots of equation (7) will have negative real parts if and only if the following conditions are satisfied:

$$\begin{cases} a_1 > 0, \\ a_3 > 0, \\ a_1 a_2 > a_3 \end{cases} \quad (10)$$

Given $a_1 > 0$, the stability of the fixed points E is influenced by the parameters $\frac{I_g}{I_0}$, α_1 and α_2. The analysis of the stability of these fixed points as a function of $\frac{I_g}{I_0}$ for two values of the non-harmonic junction parameters α_1 and α_2 is illustrated by the curves in Figure 2. Figure 2(a) shows the region where fixed points exist or do not exist. Figure 2(b) indicates that when $\alpha_1 = 0.4$ and $\alpha_2 = 0$, the system has two fixed points – one stable and the other unstable [23]. In contrast, for $\alpha_1 = 0$ and $\alpha_2 = 0.4$, the system has four fixed points, including two stable and two unstable, as illustrated in Figure 2(c) (Figure $2(b_1)$ and $2(c_1)$ show that with $\alpha_1 = 0.8$; $\alpha_2 = 0$ and $\alpha_1 = 0$; $\alpha_2 = 0.8$, the system also exhibits four fixed points, consisting of two stable and two unstable ones. The rectangular dashed curves represent the stable fixed points. It is also observed that the system consistently exhibits four fixed points when for $\alpha_2 \geq 0.4$, a condition not fulfilled when $\alpha_1 = 0.4$.

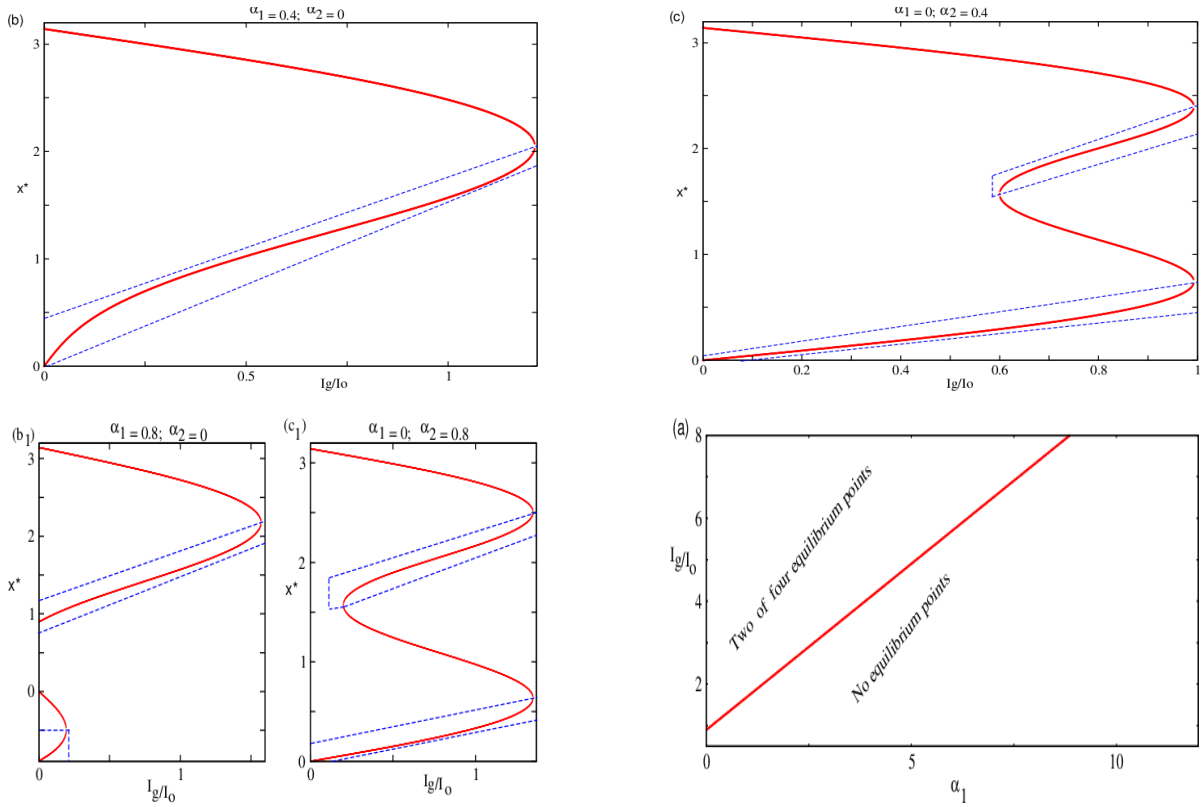

Fig. 2: A) Limit of Existence of Fixed Points in the Parameter Space Covering A_1 and Ig/I_1; B), C), B_1), C_1 Curves of the Stability or Not of the Fixed Points Compared to the Parameter Ig/I0 for A1 = 0.4; A2 = 0 and A1 = 0; A2 = 0.4 for B), C). $A_1 = 0.8$; $A_2 = 0$ and $A_1 = 0$; $A_2 = 0.8$ for B_1), C_1).

4. Bifurcation and Chaotic Oscillations

Figure 3 shows a bifurcation diagram obtained with the Runge-Kutta algorithm of order 4 method, while varying the control parameter α_1 in the range $0.27 \leq \alpha_1 \leq 0.4$ for different α_2. The other parameters are held constant at values $\varepsilon = 0.707$; $\xi = 3$ like [17] and $I_0 = 1$; $w = 1$; $E_f = 35$. As shown in Figure 5, the presence of a harmonic term of order three with a slightly high value of α_2 modifies the bifurcation diagrams. Compared to Figure 3, the only chaotic region, namely ($0.358 \leq \alpha_1 \leq 0.4$ at $\alpha_2 = 0.08$) in Figure 5, is shifted to ($0.299 \leq \alpha_1 \leq 0.317$ at $\alpha_2 = 0.2$). In addition, the width of the chaotic region is reduced by 0.024. The distance between the chaotic regions for the different values of α_2(0.08 and 0.2) shows that the third-order harmonic term significantly alters the nonlinear dynamics of the RCLSJ model of the Josephson junction. The different regular and chaotic behaviors observed in Figure 3 and Figure 5 are respectively confirmed by the phase space curves of Figure 4 and Figure 6.

Figure 7 shows the bifurcation diagrams obtained with the Runge-Kutta algorithm of order 4 using the amplitude of the current source as the control parameter, varied in the range $32 \leq E_f \leq 35$ for different values of Ig and α_2. The other parameters are held constant at values $\varepsilon = 0.735$; $\xi = 3$; $I_0 = 1$; $w = 0.95$; $\alpha_1 = 0.1$. This figure shows that the system is stable for $32 \leq E_f \leq 34.14$ and becomes chaotic for $34.14 \leq E_f \leq 35$ when $Ig = 1.188$ and $\alpha_2 = 0$. These behaviors, compared to those in Figure 9, show an expansion from $34.02 \leq E_f \leq 34.14$ in the chaotic region when the intensity of the negative conductance Ig varies from 1.188 to 1.191, while $\alpha_2 = 0$. This shows that at low values of the negative conductance intensity, the system loses energy and the chaotic dynamics transition into regular oscillations (attenuation of certain hidden modes of the system that are periodically unstable). The increase in the chaotic region also shows that the negative conductance enhances the chaotic oscillations of the excitation current at high values of its intensity, Ig. The different regular and chaotic behaviors observed in Figure 7 and Figure 9 are respectively confirmed by the phase space curves of Figure 8 and 10. Figure 11, obtained for $Ig = 1.191$ and $\alpha_2 = 0.015$, shows that the system is stable from $32 \leq E_f \leq 34.70$ and becomes chaotic beyond 34.70. These behaviors show a large reduction in the chaotic region compared to the behaviors observed in Figure 7. This again shows that the harmonic term of order three modifies the nonlinear dynamics of the RCLSJ model of the Josephson junction. These different behaviors observed are largely different from those observed in [16] when the same junction is used at the harmonic term of order two. This then shows the contribution of the third-order harmonic term and negative conductance to the dynamics of the RCLSJ model of the Josephson junction.

From a physical perspective, these mathematical results provide important insights into the actual behavior of the Josephson junction-based circuit. Stable fixed points correspond to robust operating regimes where oscillations remain periodic and predictable, ensuring controlled energy transfer with minimal losses, a condition desirable for reliable superconducting devices. Unstable fixed points and bifurcation thresholds represent critical conditions where small perturbations, such as noise or parameter fluctuations, can drastically alter the system's operation, leading to undesirable instability. Chaotic regions correspond to irregular, broadband oscillations that increase energy dissipation

and reduce coherence, which can severely limit the performance of superconducting circuits in applications such as qubits or resonant detectors. The observation that the third-order harmonic term and negative conductance reshape the chaotic regions implies that these parameters can be used as tuning knobs: reducing chaos to stabilize quantum states for quantum computation, or conversely, enhancing chaotic oscillations for applications in secure communications and random signal generation.

In the specific context of superconducting qubits, these results underline the dual role of nonlinear dynamics. Stable oscillatory regimes correspond to coherent quantum states with long lifetimes, which are essential for reliable qubit operation and quantum gate fidelity. Conversely, chaotic dynamics introduce decoherence through enhanced energy dissipation and unpredictable phase fluctuations, leading to reduced qubit performance. The ability of the third-order harmonic term (α_2) to shrink and shift chaotic regions indicates that finetuning nonlinear coupling can suppress decoherence pathways, thus preserving quantum coherence. Similarly, the modulation of chaos by negative conductance (Ig) highlights a mechanism to control energy flow within the circuit, either minimizing dissipation for quantum information storage or intentionally amplifying fluctuations for tunable microwave sources. Therefore, understanding and controlling these nonlinear effects is crucial not only for optimizing Josephson-based circuits but also for advancing the design of stable, low-dissipation superconducting qubits in practical quantum technologies

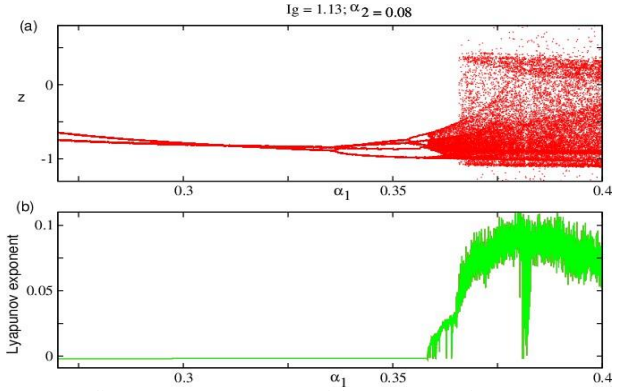

Fig. 3: Bifurcation Diagram and Its Corresponding Lyapunov Exponent of the System (3) for Ξ = 3; E = 0.707; Ω = 1; Γ = 0.01; E_F = 35; I_0 = 1.

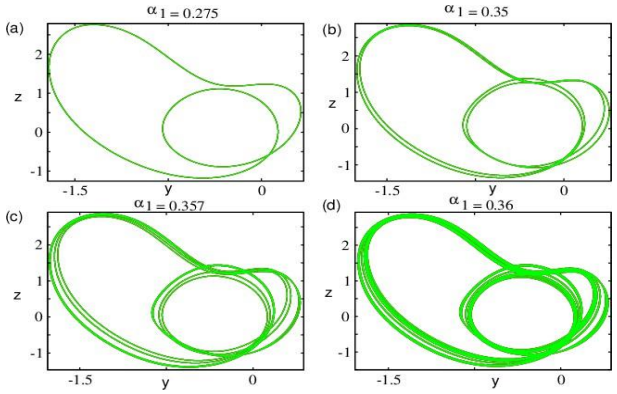

Fig. 4: Phase Portraits for A1 = 0.275; A_1 = 0.35; A_1 = 0.357 and A_1 = 0.36 Respectively of Curves (A); (B); (C) and (D) of Fig.3.

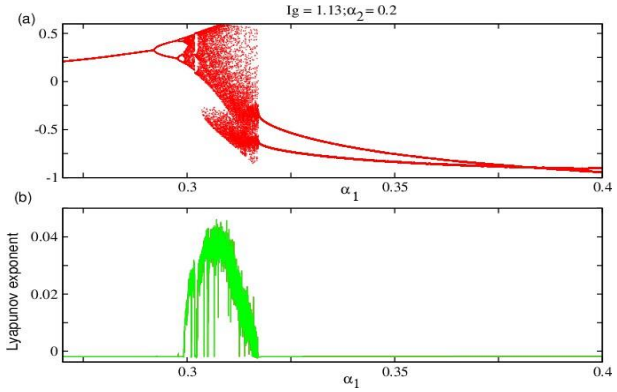

Fig. 5: Bifurcation Diagram and Its Corresponding Lyapunov Exponent of the System (3) for Ξ = 3; E = 0.707; Ω = 1; Γ = 0.01; E_F = 35; I_0 = 1.

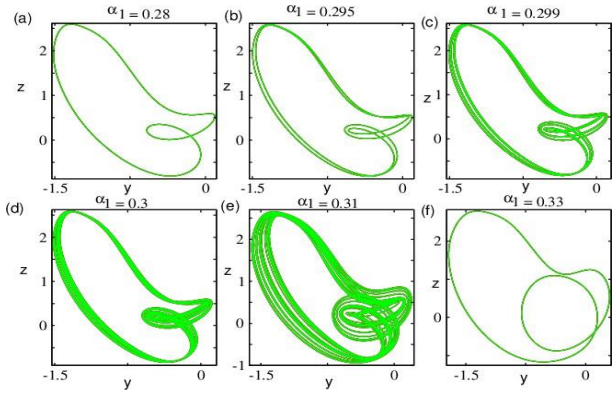

Fig. 6: Phase Portraits for $A_1 = 0.28$; $A_1 = 0.295$; $A_1 = 0.299$; $A_1 = 0.30$; $A_1 = 0.31$ and $A_1 = 0.33$ Respectively of Curves (A); (B); (C); (D); (E) and (F) of Fig.5.

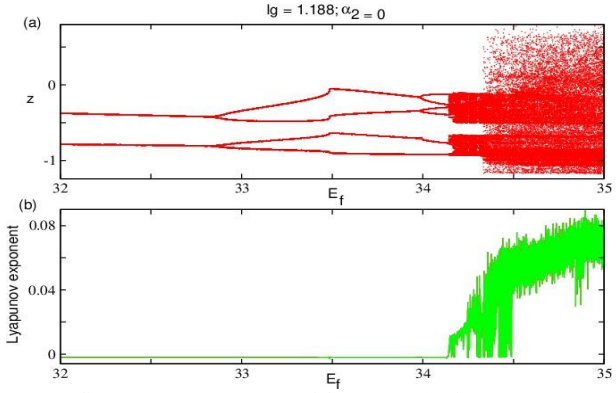

Fig. 7: Bifurcation Diagram and Its Corresponding Lyapunov Exponent of the System (3) for Ξ = 3; E = 0.735; Ω = 0.95; Γ = 0.01; $A_1 = 0.1$; $I_0 = 1$.

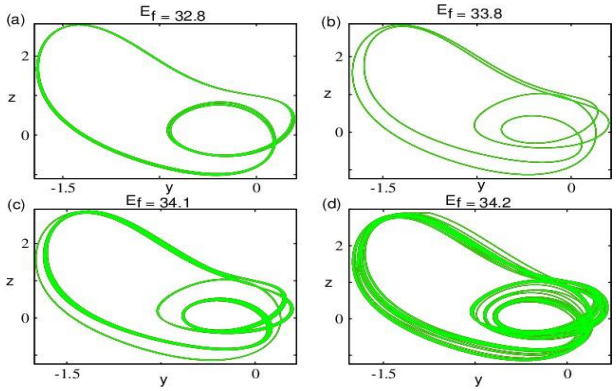

Fig. 8: Phase Portraits for $E_F = 32.8$; $E_F = 33.8$; $E_F = 34.1$ and $E_F = 34.8$ Respectively of Curves (A); (B); (C) and (D) of Fig.7.

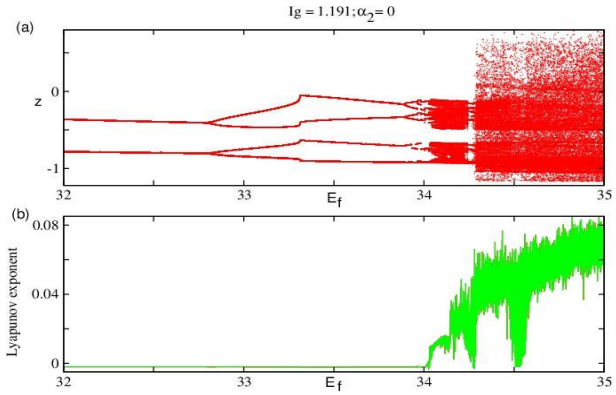

Fig. 9: Bifurcation Diagram and Its Corresponding Lyapunov Exponent of the System (3) for Ξ = 3; E = 0.735; Ω = 0.95; Γ = 0.01; A1 = 0.1; $I_0 = 1$.

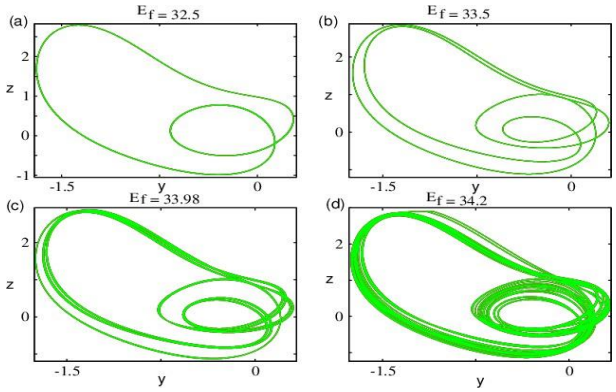

Fig. 10: Phase Portraits for $E_F = 32.5$; $E_F = 33.5$; $E_F = 33.98$ and $E_F = 34.2$ Respectively of Curves (A); (B); (C) and (D) of Fig.9.

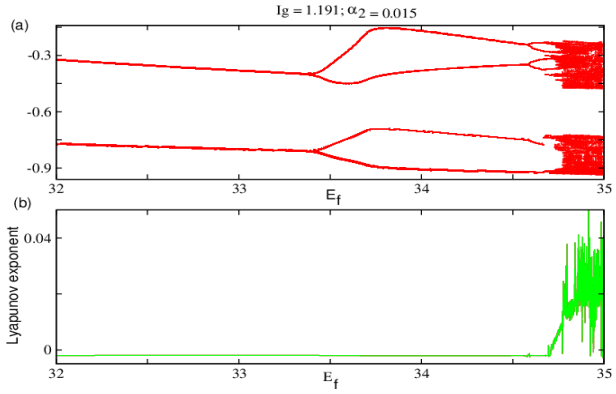

Fig. 11: Bifurcation Diagram and Its Corresponding Lyapunov Exponent of the System (3) for Ξ = 3; E = 0.735; Ω = 0.95; Γ = 0.01; $A_1 = 0.1$; $I_0 = 1$.

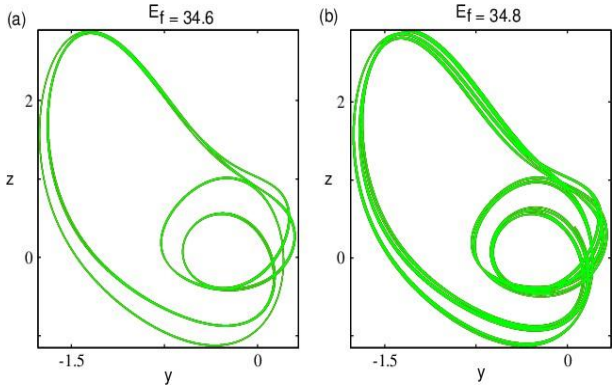

Fig. 12: Phase Portraits for $E_F = 34.S6$ and $E_F = 34.8$, Respectively, of Curves (A) and (B) of Fig.11.

5. Synchronization of The RCLSJ Junction

The objective of this section is to drive the synchronization error to zero by ensuring the global asymptotic stability of the master-slave system using the Lyapunov direct method. The two RCLSJ systems are defined such that one acts as the master (x_1, y_1, z_1) and the other as the slave (x_2, y_2, z_2), and they take the following form:

$$\begin{cases} \dot{x_i} = z_i, \\ \dot{y_i} = \frac{E_f}{\gamma}\sin(wt) + \frac{1}{\xi}(-z_i - y_i)' \\ \dot{z_i} = \frac{I}{\varepsilon}\left(y_i - \tau(z_i)z_i - \sin(x_i) + \alpha_1\sin(2x_i) - \alpha_2\sin(3x_i) + \frac{I_g}{I_0}\right). \end{cases} \tag{11}$$

With $i = 1,2$

Synchronization error

$$\begin{cases} e_1 = x_2 - x_1, \\ e_2 = y_2 - y_1, \\ e_3 = z_2 - z_1, \end{cases} \tag{12}$$

Error dynamics
From the system equations, we obtain:

$$\begin{cases} \dot{e_1} = e_3, \\ \dot{e_2} = \frac{1}{\xi}(-e_3 - e_2), \\ \dot{e_3} = f(x_1, x_2, z_1, z_2) + \mu, \end{cases} \quad (13)$$

With

$$f(x_1, x_2, z_1, z_2) = \frac{1}{\varepsilon}\left[-\tau(z2)z2 + \tau(z1)z1 + \sin(x_1) - \sin(x_2) + \alpha_1\left(\sin(2x_2) - \sin(2x_1)\right) + \alpha_2\left(\sin(3x_1) - \sin(3x_2)\right) + e_2\right]$$

Choice of the Lyapunov function
To ensure asymptotic stability and the convergence of the errors, we choose a candidate Lyapunov function of the form:

$$V_e = \frac{1}{2}e_1^2 + \frac{1}{2}e_2^2 + \frac{1}{2}e_3^2 \quad (14)$$

Derivative of V_e with respect to time
Let's use the direct derivative:

$$\dot{V}_e = \dot{e}_1 e_1 + \dot{e}_2 e_2 + \dot{e}_3 e_3 \quad (15)$$

Replacing (13) into (15), following a consistent development, we find:

$$\dot{V}_e = e_1 e_3 - \frac{1}{\xi}e_2^2 - \frac{1}{\xi}e_2 e_3 + e_3 f(x_1, x_2, z_1, z_2) + e_3 u \quad (16)$$

Choice of control law u
The idea is to cancel the $e_3 f(x_1, x_2, z_1, z_2)$ term via a corrective term in the control law.
We choose u as:
$u = -f(x_1, x_2, z_1, z_2) - k_1 e_1 - k_2 e_2 - k_3 e_3$ (17), with k_1, k_2, k_3 the gain constants.
Replacing (17) into (16), following a consistent development, we find:

$$\dot{V}_e = (1 - k_1)e_1 e_3 - \frac{1}{\xi}e_2^2 - \left(\frac{1}{\xi} + k_2\right)e_2 e_3 - k_3 e_3^2 \quad (18)$$

To simplify the derivative of the Lyapunov function and make the stability analysis more straightforward, while maintaining a physical structure consistent with the controlled system, we choose $k_1 = 1$, $k2 = 0$, and $k3 = 1$. The choice $k_1 = 1$ normalizes the primary feed-back gain, simplifying the Lyapunov derivative while preserving the physical scaling of the controlled system. Setting $k2 = 0$ eliminates certain coupling terms, reducing analytical complexity without omitting the dominant dynamics. Similarly, $k3 = 1$ normalizes the scaling of the associated feedback term, maintaining consistency with the system's energy balance. Together, these parameter choices simplify the stability analysis while retaining the essential physical behavior of the system. For this purpose, we have:

$$\dot{V}_e = -\frac{1}{\xi}e_2^2 - \frac{1}{\xi}e_2 e_3 - e_3^2$$

Let us apply Young's inequality to the cross term. For all $\theta > 0$,

$$|e_2 e_3| \leq \frac{\theta}{2}e_2^2 + \frac{1}{2\theta}e_3^2 \Rightarrow -\frac{1}{\xi}e_2 e_3 \leq \frac{1}{\xi}\left(\frac{\theta}{2}e_2^2 + \frac{1}{2\theta}e_3^2\right)$$

By bounding $\dot{V}_e$, we obtain

$$\dot{V}_e \leq \left(\frac{1}{\xi} - \frac{\theta}{2\xi}\right)e_2^2 - \left(1 - \frac{1}{2\theta\xi}\right)e_3^2$$

By setting $c_2(\theta) = \frac{1}{\xi}\left(1 - \frac{\theta}{2}\right)$, $c_3(\theta) = 1 - \frac{1}{2\theta\xi}$.
We have

$$\dot{V}_e \leq -c_2(\theta)e_2^2 - c_3(\theta)e_3^2$$

To ensure $c_2(\theta) > 0$, and $c_3(\theta) > 0$ it is necessary to

$$1 - \frac{\theta}{2} > 0 \Rightarrow 0 < \theta < 2,$$

$$1 - \frac{1}{2\theta\xi} > 0 \Rightarrow \theta > \frac{1}{2\xi}$$

Then $\xi > \frac{1}{4}$

- if $\xi > \frac{1}{4}$ there exists $\theta \in \left(\frac{1}{2\xi}, 2\right)$ (therefore $c2(\theta), c3(\theta) > 0$) and we have $\dot{V}_e \leq 0$ therefore, negative definite ;
- if $\xi = \frac{1}{4}$ the interval is reduced, and we obtain semi-negativity;

- if $\xi < \frac{1}{4}$ there does not exist a θ satisfying both inequalities, and Young's inequality, without further modification, does not guarantee $\dot{V}_e \leq 0$.

u become:

$$u = \frac{1}{\varepsilon}\left[\tau(z2)z2 - \tau(z1)z1 - \sin(x_1) + \sin(x_2) - \alpha_1\left(\sin(2x_2) - \sin(2x_1)\right) - \alpha_2\left(\sin(3x_1) - \sin(3x_2)\right) - e_2\right] - e_1 - e_3$$

Based on Equation (14), when ξ is greater than or equal to one-fourth, the error signal V_e maintains a positive value while $\dot{V}_e$ is negative or semi-negative, ensuring asymptotic convergence and thereby achieving complete synchronization between the master and slave systems.

5.1. Fixed Points and Stability

The control law:

$$u = \frac{1}{\varepsilon}\left[\tau(z2)z2 - \tau(z1)z1 - \sin(x_1) + \sin(x_2) - \alpha_1\left(\sin(2x_2) - \sin(2x_1)\right) - \alpha_2\left(\sin(3x_1) - \sin(3x_2)\right) - e_2\right] - e_1 - e_3 \quad (21)$$

So we have:

$$u = -f(x_1, x_2, z_1, z_2) - e_1 - e_3 \quad (22)$$

Substituting (22) into (13), we find:

$$\begin{cases} \dot{e_1} = e_3, \\ \dot{e_2} = \frac{1}{\xi}(-e_3 - e_2), \\ \dot{e_3} = -e_1 - e_3, \end{cases} \quad (23)$$

- Fixed points

The fixed points are defined by:

$$\dot{e_1} = \dot{e_2} = \dot{e_3} = 0.$$

We solve

$$\begin{cases} e_3 = 0, \\ -e_3 - e_2 = 0, \\ -e_1 - e_3 = 0, \end{cases}$$

So the origin $M_0 \begin{pmatrix} 0 \\ 0 \\ 0 \end{pmatrix}$ is the only fixed point of the system (23)

- Stability analysis

The system (23) is already linear, so we can directly analyze its Jacobian matrix:

$$A = \begin{pmatrix} 0 & 0 & 1 \\ 0 & \frac{-1}{\xi} & \frac{-1}{\xi} \\ -1 & 0 & -1 \end{pmatrix}_{M_0} \quad (24)$$

The characteristic polygon gives:

$$\det(A_{Mo} - \lambda I) = \begin{vmatrix} -\lambda & 0 & 1 \\ 0 & -\left(\lambda + \frac{1}{\xi}\right) & \frac{-1}{\xi} \\ -1 & 0 & -(1+\lambda) \end{vmatrix} \quad (25)$$

After canceling the characteristic polynomial, we find the following eigenvalues:

$$\begin{cases} \lambda_1 = \frac{-1}{\xi}, \\ \lambda_2 = \frac{-1+i\sqrt{3}}{2}, \\ \lambda_3 = \frac{-1+i\sqrt{3}}{2}, \end{cases} \quad (26)$$

The fixed point at the origin is a stable focal node (or a three-dimensional attractive focal point). The dynamics of the considered system, characterized by a triplet of eigenvalues with strictly negative real parts, correspond to an asymptotically stable linear system, admitting a focal attractor at the origin. An appropriate choice of coupling parameters ($k_1 = 1, k_2 = 0, k_3 = 1$) leads to an exponential convergence of the synchronization error to zero. Thus, complete synchronization between the two systems is asymptotically achieved. A numerical confirmation of this result is presented below using the fourth-order Runge-Kutta method, for a range of values of the negative conductance intensity and the second-order anharmonic term of the junction.

Figures 13 and 14 show the synchronization of the system in the absence of negative conductance when $\alpha_2 = 0.015$. The state variables of the master and slave systems follow each other and coincide (figure 13) while all errors converge to zero (figure 14) when the controller value is greater than or equal to 270. Figures 15 and 16 show the same behavior when $\alpha_2 = 2$. By comparing these curves, we observe a modification in the synchronization frequency when α_2 increases from 0.015 to 2. This demonstrates that the third-order harmonic term modifies the synchronization frequencies by introducing new resonance modes. These different behaviors are markedly different from those reported in [16], where the same junction was used with a second-order harmonic term. This highlights the specific contribution of the third-order harmonic term to the dynamics of the RCLSJ Josephson junction model.

Figures 17 and 18 show the synchronization of the system in the presence of negative conductance and the harmonic term of order three when Ig = 1.191 and $\alpha_2 = 0.015$. The state variables of the master and slave systems follow each other and coincide (figure 17), and all errors converge to zero (figure 18) when the controller value is greater than or equal to 270. Compared with Figures 13, these results show that increasing the intensity of the negative conductance from 0 to 1.191, while keeping $\alpha_2 = 0.015$, enhances higher-frequency oscillations.

Synchronization of the system when I_g=0 and α_2=0.015.

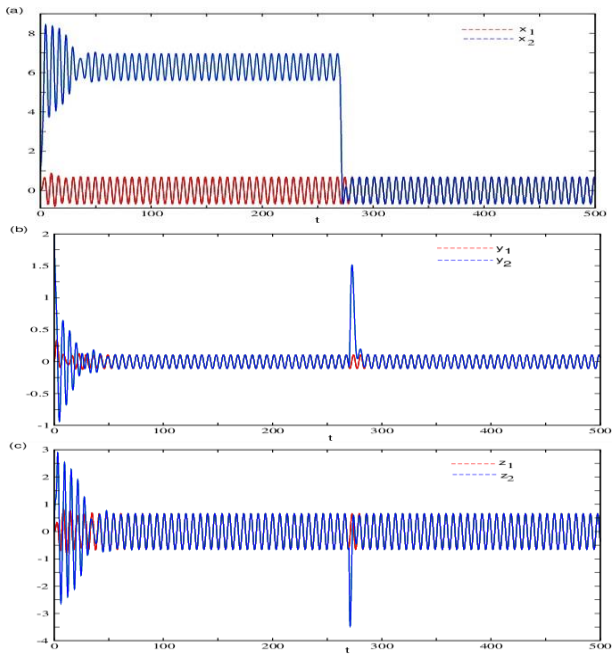

Fig. 13: Time Stories of the Systems 11 Synchronization Variables for X_1 and X_2, Y_1 and Y_2 and Z_1 and Z_2. the Parameters of Simulation Are: $\Xi = 3$; $E = 0.735$; $I_0 = 1$; $\Omega = 0.95$; $\Gamma = 0.01$; $E_f = 33$; $A_1 = 0.1$ with Initial Conditions: $(X_1(0); Y_1(0); Z_1(0)) = (0; 0; 0)$ and $(X_2(0); Y_2(0); Z_2(0)) = (1; 2; 0)$ for the Systems 11. When the Controller Is Applied at the Date $T \geq 270$s, the Slave System follows the Master System.

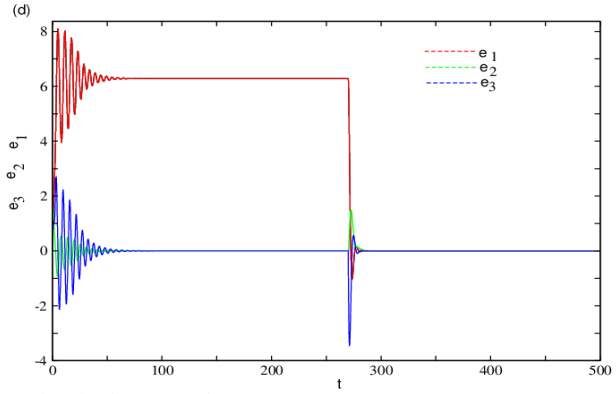

Fig. 14: Time Stories of the Systems 11 Synchronization Errors for $\Xi = 3$; $E = 0.735$; $I_0 = 1$; $\Omega = 0.95$; $\Gamma = 0.01$; $E_f = 33$; $A_1 = 0.1$ with Initial Conditions: $(X_1(0); Y_1(0); Z_1(0)) = (0; 0; 0)$ and $(X_2(0); Y_2(0); Z_2(0)) = (1; 2; 0)$ for the Systems 11. When the Controller Is Applied at the Date $T \geq 270$s, the Synchronization Error Tends to zero.

Synchronization of the system when Ig 0and α_2=2.

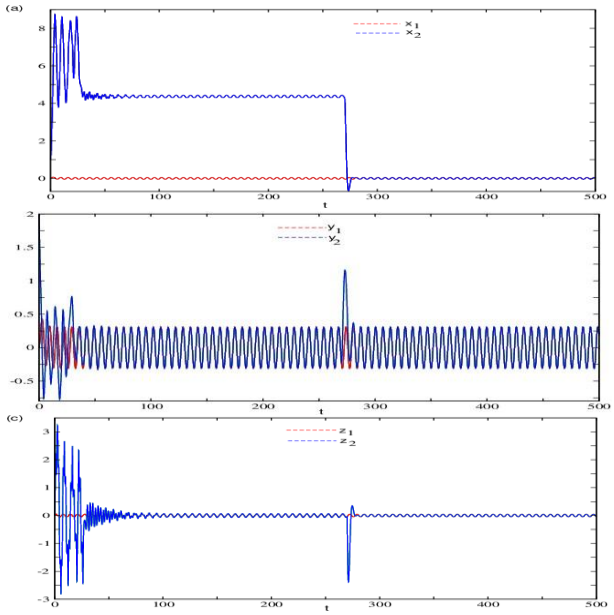

Fig. 15: Time Stories of the Systems 11 Synchronization Variables for X_1 and X_2, Y_1 and Y_2 and Z_1 and Z_2. the Parameters of Simulation Are: $\Xi = 3$; $E = 0.735$; $I_0 = 1$; $\Omega = 0.95$; $\Gamma = 0.01$; $E_f = 33$; $A_1 = 0.1$ with Initial Conditions: $(X_1(0); Y_1(0); Z_1(0)) = (0; 0; 0)$ and $(X_2(0); Y_2(0); Z_2(0)) = (1; 2; 0)$ for the Systems 11. When the Controller Is Applied at the Date $T \geq 270s$, the Slave System follows the Master System.

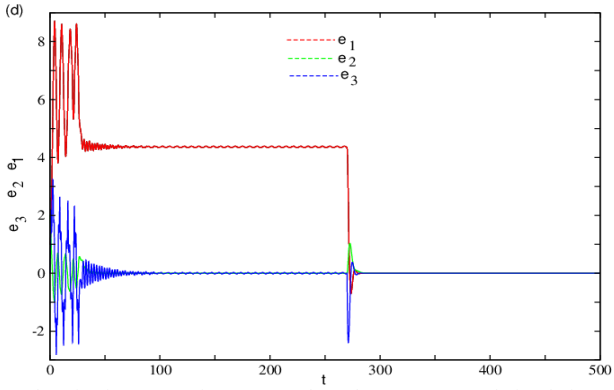

Fig. 16: Time Stories of the Systems 11 Synchronization Errors for E_1; E_2 and E_3. the Parameters of Simulation Are: $\Xi = 3$; $E = 0.735$; $I_0 = 1$; $\Omega = 0.95$; $\Gamma = 0.01$; $E_f = 33$; $A_1 = 0.1$ with Initial Conditions: $(X_1(0); Y_1(0); Z_1(0)) = (0; 0; 0)$ and $(X_2(0); Y_2(0); Z_2(0)) = (1; 2; 0)$ for the Systems 11. When the Controller Is Applied at the Date $T \geq 270s$, The Synchronization Error Tends to zero.

Synchronization of the system when Ig 1.191 and α_2=0.015.

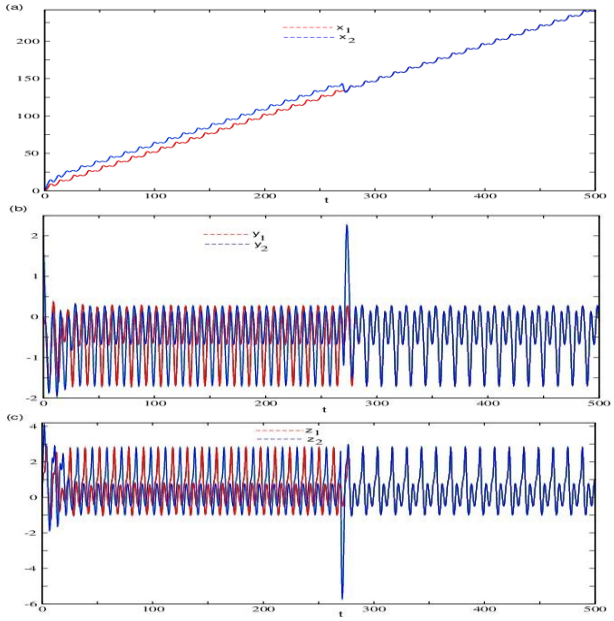

Fig. 17: Time Stories of the Systems 11 Synchronization Variables for X1 and X_2, Y_1 and Y_2 and Z_1 And Z_2. the Parameters of Simulation Are: $\Xi = 3$; $E = 0.735$; $I_0 = 1$; $\Omega = 0.95$; $\Gamma = 0.01$; $E_f = 33$; $A_1 = 0.1$ with Initial Conditions: $(X_1(0); Y_1(0); Z_1(0)) = (0; 0; 0)$ and $(X_2(0); Y_2(0); Z_2(0)) = (1; 2; 0)$ for the Systems 11. When the Controller Is Applied at the Date $T \geq 270s$, the Slave System follows the Master System.

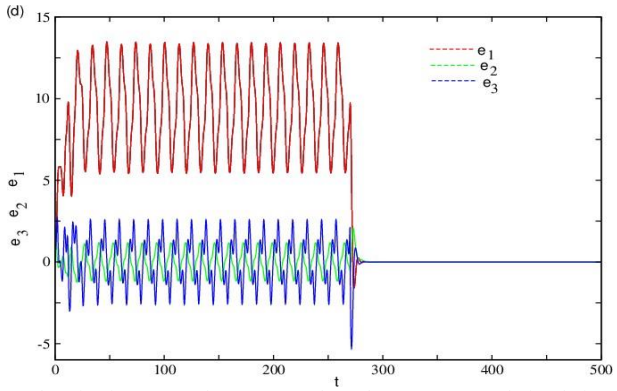

Fig. 18: Time Stories of the Systems 11 Synchronization Errors for E_1; E_2 And E_3. the Parameters of Simulation Are: $\Xi = 3$; $E = 0.735$; $I_0 = 1$; $\Omega = 0.95$; $\Gamma = 0.01$; $E_f = 33$; $A_1 = 0.1$ with Initial Conditions: $(X_1(0); Y_1(0); Z_1(0)) = (0; 0; 0)$ and $(X_2(0); Y_2(0); Z_2(0)) = (1; 2; 0)$ for the Systems 11. When the Controller Is Applied at the Date $T \geq 270s$, the Synchronization Error Tends to Zero.

6. Conclusions

Theoretical and numerical analysis of the RCLSJ model (Resistively, Capacitively, and Inductively Shunted Junction) modeled by a nonlinear current source with a current-phase relationship $I_0(\sin x - \alpha_1 \sin 2x + \alpha_2 \sin 3x)$ coupled to a negative conductance are studied in this paper. The rate equations describing the RCLSJ model do not have fixed points for some regions but admit two (when $\alpha_1 = 0.4$ and $\alpha_2 = 0$) or four (when $\alpha_1 = 0.8$ and $\alpha_2 = 0$) and (when $\alpha_1 = 0$ and $\alpha_2 \geq 0.4$) fixed points for other regions covering the negative conductance intensity and the second-order harmonic term of the junction when the critical junction intensity is normalized. The presence of a third-order harmonic term with a slightly high α_2 value modifies the bifurcation diagrams. This induces a shift in the chaotic region of the model studied. We therefore deduce that the harmonic term of order three modifies the nonlinear dynamics of the RCLSJ model of the Josephson junction. We have shown that at low values of the negative conductance intensity, the system loses energy and the chaotic dynamics become regular (attenuation of certain hidden orders of the system, which present periodically unstable modes). At a high value of the intensity of the negative conductance, we note an increase in the chaotic region; this shows that the negative conductance reinforces the oscillations of the excitation current. Compared to what was done in [23], this new paper shows that the negative conductance behaves like a multi-periodic pulse source when the same RCLSJ model is used, but with a second-order harmonic term. It supplies energy to the system instead of absorbing it as its intensity increases. We have also shown that the third-order harmonic term modifies the synchronization frequencies by introducing new resonance modes, and the negative conductance enhances an increase in the frequency oscillations. In view of the important results of this work, a follow-up study could be proposed to experimentally verify the shift in synchronization frequencies observed numerically. This experiment would use a Josephson junction circuit with tunable negative conductance, allowing precise control of the system's nonlinear parameters. Such a setup would enable validation of the effects of negative conductance on synchronized dynamics and resonance modes, paving the way for controlled applications in superconducting electronics.

References

[1] Gu, X., Kockum, A. F., Miranowicz, A., Liu, Y., Nori, F.: Microwave photonics with superconducting quantum circuit. Physics Reports. 718-719 (2017). https://doi.org/10.1016/j.physrep.2017.10.002.
[2] Bunyk, P. I., et al.: Architectural considerations in the design of a superconducting quantum annealing processor. IEEE Transactions on Applied Superconductivity 24, (2014). https://doi.org/10.1109/TASC.2014.2318294.
[3] Hwang, S., et al.: Type-I superconductor pick-up coil in superconducting quantum interference device-based ultra-low field nuclear magnetic resonance. Applied Physics Letters. 104, 6 (2014). https://doi.org/10.1063/1.4865497.
[4] Belykh, V. N., Pedersen, N. F., Soerensen O. H.: Shunted Josephson junction model II. The nonautonomous case. Phys. Rev B. 16, 4860 (1977). https://doi.org/10.1103/PhysRevB.16.4860.
[5] Belykh, V. N., Pedersen, N. F., Soerensen O. H.: Shunted Josephson junction model I. The autonomous case. Phys. Rev B. 16, 4853 (1977). https://doi.org/10.1103/PhysRevB.16.4853.
[6] Crutchfield, J. P., Farmer, J. D., Huberman, B. A.: Properties of fully developed chaos in one-dimensional maps. Phys. Rep. 92(2), 45 (1982). https://doi.org/10.1016/0370-1573(82)90089-8.
[7] Likharev, K. K.: Dynamics of Josephson junctions and circuits. Springer, New York (1986).
[8] Dana, S. K., Sengupta D. C., Edoh, D. K.: Chaotic dynamics in Josephson junction. IEEE Trans. Circuit Syst. I 48, 990 (2001). https://doi.org/10.1109/81.940189.
[9] Whan, C.B., Cawthorne A. B, Lobb, C. J.:Synchronization and phase locking in two-dimensional arrays of Josephson junction. Phys. Rev. B. 53, 12340 (1996). https://doi.org/10.1103/PhysRevB.53.12340.
[10] Cawthorne A. B, Whan, C.B., Lobb, C. J: Complex dynamics of resistively and inductively shunted Josepson junction. J. Apll. Phys. 84,1126-1132 (1998). https://doi.org/10.1063/1.368113.
[11] Yang, X. S., Li, Q. Chaos Solitons Fractals 27, 25 (2006). https://doi.org/10.1016/j.chaos.2005.04.017.
[12] Wu, D. W., Liu, C. R. J. Eng. Ind. 107,107 (2014).
[13] Chen, D. Y., Zhao, W. L., Ma, X. Y., Zhang, R. F. Comput. Math Appl. 61, 3161 (2011). https://doi.org/10.1016/j.camwa.2011.04.010.
[14] Chen, D. Y., Zhang, R. F., Ma, X. Y., Liu, S. Nonlinear Dyn. 69, 35 (2011). https://doi.org/10.1007/s11071-011-0244-7.
[15] Chen, D. Y., Shi, L., Chen, H. T. Ma, X. Y. Nonlinear Dyn. 67, 1745 (2012). https://doi.org/10.1007/s11071-011-0102-7.
[16] Oseni, C. O. A., Monwanou, A. V.: Identical and reduced-order synchronization of some Josephson junction model. Eur. Phys. J. B. 95, 197 (2022). https://doi.org/10.1140/epjb/s10051-022-00462-2.
[17] Likharev, K. K.: Dynamics of Josephson junctions and circuits Gordon and breach. New York. 92.
[18] Ling, F. Y., Shen K.: Synchronization of chaos in resistive-capacitive-inductive shunted Josephson junctions. Chin. Phys. B 2 17, 550 (2008). https://doi.org/10.1088/1674-1056/17/2/033.
[19] Kakpo, M. A., Miwadinou, C. H.: Control of the chaotic dynamics of the RCLSJ model of the Josephson junction by the frequency of an excitation current and the internal resistance of a coil. Phys. Scr. 99, 085202 (2024). https://doi.org/10.1088/1402-4896/ad4ff0.
[20] Yokoi, M. et al.: Negative resistance state in superconducting $NbSe_2$ induced by surface acoustic waves. SCIENCE ADVANCES.,6, 1377 (2020). https://doi.org/10.1126/sciadv.aba1377.

[21] Sergey, K. et al.: Band-selective third-harmonic generation in superconducting MgB_2: Possible evidence for Higgs amplitude mode in the dirty limit . Phys. Rev. B 104, L140505 (2021).
[22] Seibold, G. et al.: Third-harmonic generation from collective modes in disordered superconductors. Phys. Rev. B 103, 014512 (2021). https://doi.org/10.1103/PhysRevB.103.014512.
[23] Pomalegni, G. F., Kakpo, M. A., Miwadinou, C. H.: Nonlinear dynamics and synchronization of an excited Josephson junction. J. Nonlinear Sci. Apll., 18, 225-238 (2025. https://doi.org/10.22436/jnsa.018.04.01.